Hetero- and low-dimensional structures

Silicon nanowire arrays synthesized using the modified MACE process: Integration into chemical sensors and solar cells

M.G. Dusheiko, V.M. Koval, T.Yu. Obukhova

National Technical University of Ukraine "Igor Sikorsky Kyiv Polytechnic Institute",
Microelectronic department
37, prospect Peremohy, 03056 Kyiv, Ukraine
E-mail: t.y.obukhova@gmail.com; pvlab_kpi@ukr.net

Abstract. In this work, the influence of the technological process for metal-assisted chemical etching on surface morphology and electrophysical properties of obtained nanostructures has been investigated. It has been demonstrated that the obtained structures with a high aspect ratio could be used both in sensors and solar cells. It has been shown that application of the metal-assisted chemical etching (MACE) process enables to significantly improve the short-circuit current density in silicon solar cells (up to 29 mA/cm^2). Also, the possibility of detection of hydrogen peroxide and glucose (*via* enzymatic reaction) by resistor-like sensors with nanostructured silicon as the sensitive area has been demonstrated with the sensitivity up to 2.5…2.75 mA/V·%.

1. Introduction

Silicon nanostructures, in particular nanowires (NWs) with high aspect ratio, attract great interest during recent decades due to unique properties and a wide range of large possibilities to be applied in modern devices [1–5]. In each case of using the Si NWs, certain nanostructure properties are required, *i.e.*, a large surface area for better light trapping in actuators or an increase in surface sensitive properties in sensors.

Nanostructures can be fabricated using bottom-up or top-down approaches. The second one is simpler and more suitable for industrial applications [6]. In the case of Si nanostructures, two different technologies are commonly used: dry and wet etching [7, 8]. The metal-assisted chemical etching (MACE), as a kind of wet chemical etching, is very promising for obtaining Si nanowires (Si NWs) with a high aspect ratio [9, 10]. The mechanism of synthesis of Si NWs by using this method consists of two stages [11, 12]. At the first stage, metal nanoparticles (NPs), *e.g.*, Ag NPs precipitate on Si surface, and then chemical etching of Si material occurs with metal NPs acting as a catalyst. The etching rate of Si wafer increases significantly in the vicinity of metal NPs. The depth of etched grooves is determined by the chemical composition of solutions and the duration of both stages in MACE. So, the advantages of the MACE technique are simplicity of implementation, low cost and

formation of nanostructures with a high aspect ratio, such as arrays of NWs and nanoholes [13, 14]. A lot of reports on Si NWs obtained using MACE are aimed at the structural investigation without device application [15–20], however, the understanding of correlation between the structural and optical properties and the real device characteristics is crucial to promote further development of NW-based actuators and sensors.

In this work, we synthesize Si NWs by means of MACE for further application in solar cells and chemical sensors. To reach the best results in ascertaining the influence of etching process parameters on device characteristics, we carried out preparation of various sets of samples. The photovoltaic (PV) characteristics were measured using the MACE Si solar cells and chemical sensors aimed at H$_2$O$_2$ detection.

2. Experimental details

2.1. MACE technique

Monocrystalline Si(100) wafers of *p*-type conductivity with a resistivity close to 1 Ω·cm were used for sample preparation. The wafer cleaning process consisted of three standard RCA steps – cleanup in piranha solution, RCA-1, and RCA-2. To remove contamination, the piranha solution (H$_2$SO$_4$:3H$_2$O) was used at 100 °C for 15 min. Then the wafer cleaning was carried out using RCA-1 (H$_2$O$_2$:NH$_4$OH:3H$_2$O) at 80 °C for 10 min.

Table 1. Samples series.

Sample	Metal	t_1, s	Nitrate nanopowder, mg	t_2, min	H_2O_2, ml
Ag1	Ag	20	68	30	0.4
Ag2				90	
Ag3				150	
Ag4				30	0.8
Ag5				90	
Ag6				150	
Ag7		10	68	30	0.8
Ag8		20			
Ag9		40			
Ag10		60			
Ag11		20	34		
Ag12		60			
Ag13		10	68	40	0.8
Ag14				50	
Ag15				90	
Ag16		15		40	
Ag17				50	
Cu1	Cu		375	30	2
Cu2				40	
Cu3				50	
Au1	Au		40…50 nm	50	0.8

The next step was metal contamination removal in RCA-2 (H_2O_2:HCl:$3H_2O$) at 80 °C for 10 min. Each step was finished by rinsing in a three-cascading bath of deionized water at different temperatures (60, 40 and 20 °C). Then the wafers were dried in a centrifuge and subjected to MACE technique immediately. In this work, three techniques of MACE were used: (1) the two-stage process with Ag NPs, (2) the one-stage process with Cu NPs, and (3) etching with previously synthesized Au NPs.

(1) MACE with Ag NPs. The first stage of MACE process consists in the deposition of Ag NPs from AgNO₃-based solution on the Si surface. To prepare this solution, a certain amount of AgNO₃ nanopowder (34, 68 or 136 mg) was dissolved in 10 ml of H_2O, and 40% HF solution (4.42 ml) was added. Then H_2O was added to the mixture to obtain 20 ml of solution. Si wafers were immersed in the prepared solutions at room temperature for 10, 40 or 60 s (duration of the first stage of MACE). The second stage of MACE consists of the etching of Si surface in the vicinity of Ag NPs in H_2O_2-based solution. To prepare the solution, 30 ml of H_2O was mixed with a certain amount of H_2O_2 (0.4, 0.8 or 1.6 ml), and 11 ml of 40% HF solution was added. Then H_2O was added to the mixture to obtain 50 ml. The etching process was carried out at room temperature for 30, 90 or 150 min (duration of the second stage of MACE). Then Si substrates were cleaned in deionized water and dried in a centrifuge.

(2) MACE with Cu NPs. A solution was prepared as being based on Cu(NO₃)₃ nanopowder by dissolving 375 mg in 2 ml of H_2O_2 and 40% HF (25 ml). Then H_2O was added to the mixture to obtain 100 ml of solution. Si wafers were immersed in the prepared solution at room temperature from 30 to 50 min, then cleaned in deionized water and dried in a centrifuge.

(3) MACE with Au NPs. Au NPs of the size 40 to 60 nm were previously prepared by chemical synthesis from Au citrate. The solution with Au NPs spread by drop deposition on the Si surface and air-dried. At the second stage of the etching of Si surface, a solution was prepared by mixing 0.81 ml of H_2O_2 and 20.8 ml of 40% HF, then H_2O was added to obtain 100 ml of solution. The etching time varied from 30 to 60 min at room temperature. Then the wafers were cleaned and dried.

2.2. Samples

In this work, the series of 20 samples with different preparation conditions were used (Table 1).

2.3. Fabrication of solar cells

Fabrication of solar cells on the base of MACE-modified Si substrates started with the removal of Ag NPs residues from the surface. At the next stage, formation of *p-n* junction was performed using a diffusion of phosphorus dopant. This technological operation was carried out in

the diffusion furnace SMDS 3M from a liquid source. The rear contact was deposited using RF magnetron sputtering of an Al target using a Cathode 1. To form the front point contacts, a two-layered Ti/Ni metal layer was acquired by electron-beam evaporation, employing the E-beam evaporator UVD-74P-3. Then transparent conductive ITO thin film was deposited on the front side of the solar cell by RF magnetron sputtering. The structure of the solar cell based on the MACE-modified Si substrate is shown in Fig. 1.

2.4. Sensor structures fabrication

Sensor structures were formed in a standard resistor-like configuration. Ti-Ni contact grid was deposited by electron-beam evaporation through a foil mask, using the E-beam evaporator UVD-74P-3. To evaluate the metal NPs contribution to device sensitivity, half of the samples were subjected to the removal of metal NP residues from the surface. For this purpose, the samples with Ag NPs were submerged in concentrated HNO_3 for 8 hours and then washed and dried. For the samples with Cu NPs, two removal techniques were used: fast cleaning (1 min in concentrated HNO_3) and long-term cleaning (one hour in HNO_3). Au NPs were not removed because of toxicity of the process.

2.5. Characterization techniques

Surface morphology of the MACE-modified Si substrates was investigated by atomic force microscopy (AFM) in contact mode and scanning electron microscopy (SEM). The chemical analysis of Si substrate after MACE was carried out by means of energy-dispersive X-ray (EDX) spectroscopy. Optical reflectance spectra for the MACE Si substrates were recorded using a spectrophotometer. PV characteristics were measured under irradiation with simulated sunlight spectrum AM1.5.

3. Results and discussion

3.1. Chemistry of MACE of Si

According to the general MACE model [21], the oxidant is mainly reduced at the surface of metal NPs, and holes are injected from metal into Si, or electrons are transferred from Si into metal. In this way, Si surface around metal NPs has the maximum hole concentration, and dissolution of Si occurs mainly under NPs in (100) direction [22–24].

The chemistry of the two-stage Ag-MACE process can be described as two simultaneous microscopic electrochemical reactions. At the first stage, Ag^+ cations reduced on the surface act as an oxidizer for Si, while F^- ions act as complexing agents for Si products [25]:

cathode reaction: $Ag^+ + e^- \rightarrow Ag$,

anode reaction: $Si + 6F^- \rightarrow SiF_6^{2-} + 4e^-$,

overall reaction: $4Ag^+ + Si + 6F^- \rightarrow 4Ag + SiF_6^{2-}$.

At the second stage, the Si dissolution process may occur in two possible ways, depending on the number of holes per dissolved Si atom [22, 26]:
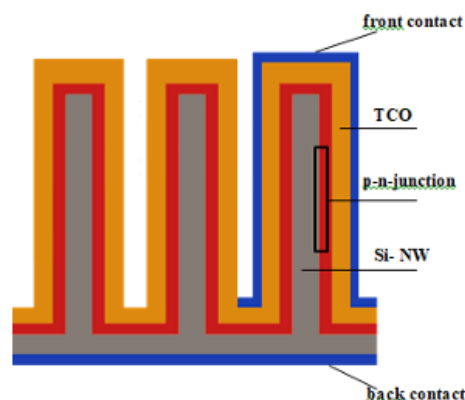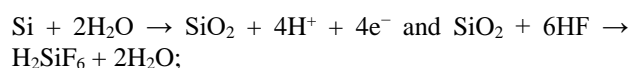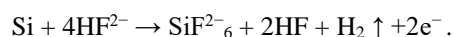

Fig. 1. Scheme of the solar cell based on MACE Si substrate: Al back contact / *p*-Si NWs / *n*-Si layer / ITO / Ti-Ni front contact.

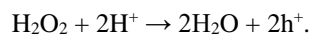1) oxidation of Si, followed by dissolution of the oxide (isotropic etching):

$Si + 2H_2O \rightarrow SiO_2 + 4H^+ + 4e^-$ and $SiO_2 + 6HF \rightarrow H_2SiF_6 + 2H_2O$;

2) direct dissolution of Si to H_2SiF_6, with H_2 evolution (anisotropic etching):

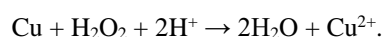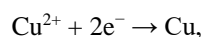$Si + 4HF^{2-} \rightarrow SiF^{2-}_6 + 2HF + H_2 \uparrow + 2e^-$.

At this stage, H_2O_2 plays the role of an oxidizing agent, which increases hole injection into Si in the vicinity of metal catalysts [23, 26]:

$H_2O_2 + 2H^+ \rightarrow 2H_2O + 2h^+$.

In the case of Cu NPs, reactions are almost the same, but Cu provides two holes [27].
For Cu redox process:

$Cu^{2+} + 2e^- \rightarrow Cu$,

$Cu + H_2O_2 + 2H^+ \rightarrow 2H_2O + Cu^{2+}$.

The Si etching in the Cu-MACE process occurs in the same way as for the Ag-MACE process described above.

As MACE is a multiple-stage process, it can be controlled in wide limits by the stage duration and concentration of solution components. In this work, some interrelations between the MACE conditions and resulting structure properties for PV and sensor applications were analyzed.

3.2. Influence of metal NP deposition conditions

The surface density of metal NPs can be controlled by both the metal nitrate concentration and the first stage duration of two-stage MACE process. The second stage of MACE (Si etching) was carried out under the same conditions (H_2O_2 volume of 0.8 ml, etching time 90 min). The increase in Ag NPs deposition time from 20 to 60 s at the same content of $AgNO_3$ (68 mg) led to changes in surface morphology (Fig. 2).

Dusheiko M.G., Koval V.M., Obukhova T. Yu. Silicon nanowire arrays synthesized using the modified MACE …
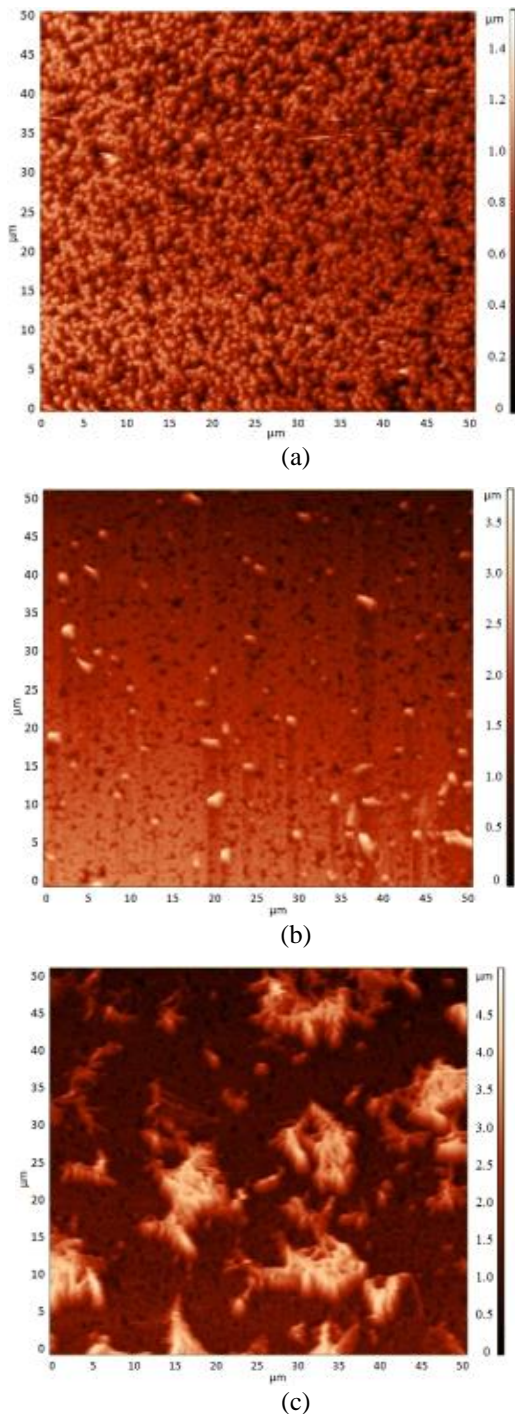
(a)

(b)

(c)

Fig 2. AFM images of Si surface with NWs MACE-prepared at different durations of Ag NPs deposition: (a) 10 s (Ag7), (b) 40 s (Ag9), (c) 60 s (Ag10). The concentration of $AgNO_3$ in solution was the same (68 mg). MACE etching conditions were as follows: $H_2O_2 – 0.8$ ml, etching time – 90 min.

From the AFM image in Fig. 2a, it can be seen that Ag deposition for 20 s results in appearance of well-pronounced nanostructures with the average height of 794 nm and the RMS value of roughness of 230 nm. The increase in Ag deposition time twice, up to 40 s, leads to formation of a larger amount of Si nanostructures merged in groups, as well as the appearance of second-phase

inclusions (bright elongated spots in Fig. 2b). The average height is 1470 nm, and RMS value of roughness is 442 nm. The significant increase in structural parameters is apparently due to the appearance of second-phase inclusions. A further increase in Ag deposition time leads to formation of compactly located Si nanostructures, as well as to the growth of dendrites over Si NWs (Fig. 2c). In this case, the average height of nanostructures is 1812 nm, and RMS value of roughness is 915 nm.

The form and chemical composition of dendrites were studied using SEM and EDX spectroscopy. Dendritic formations on Si surface look like separate sticks and agglomerates of them (Ag branches). EDX spectroscopy of the MACE surface showed that Si surface contains Ag. The quantitative chemical analysis was made for two points of the surface (in the vicinity of Ag branches and without them). It was found that there are 99.46 at.% Si and 0.54 at.% Ag at the point 1 and 87.9 at.% Si and 12.1 at.% Ag at the point 2. It follows that the branched formations, observed on the SEM image, are indeed Ag dendrites.

Besides, the influence of $AgNO_3$ content in the first solution (34, 68, and 136 mg) on the surface morphology of Si after the MACE process was studied. For this study, the second stage of MACE was carried out under the same conditions (H_2O_2 amount 0.8 ml, etching time 90 min). It was found that in the case of low $AgNO_3$ content in solution (34 mg), Ag deposition even for 60 s did not lead to precipitation of the Ag phase. For the first solution with a higher content of $AgNO_3$ (68 mg), deposition time of 40 s caused the growth of Ag "sticks" on Si surface (Fig. 2b). Duration of deposition 60 s provided formation of branched Ag dendrites (Fig. 2c). With the excess of $AgNO_3$ in the first solution (136 mg), the appearance of Ag inclusions in the form of "sticks" was observed even for Ag deposition time of 20 s, while deposition for 40 s led to more developed dendritic structure in the form of "twigs".

The metal type also influences on surface morphology (Fig. 3). In the case of the same Si etching time (second stage) the most developed and rough surface was obtained with Cu NPs (Fig 3c), while with Au NPs (Fig. 3a) surface remained almost smooth. This can be explained both by metal chemical properties (Au is more inert than Ag or Cu, and Cu is more active than Ag because of two valent electrons) and by the lower density of Au NPs on the surface, which can be observed using SEM.

3.3. Influence of Si etching conditions

While the surface pattern is determined rather by metal NPs density and their type, the depth (or height) depends on Si etching parameters (etching time and solution composition).

From SEM images in Fig. 4, it can be seen that etching time increase from 30 to 90 min leads to more developed surface morphology of Si. The structure shown in Fig. 4 was obtained not only with etching in depth of Si plate but also with lateral etching of Si NWs.
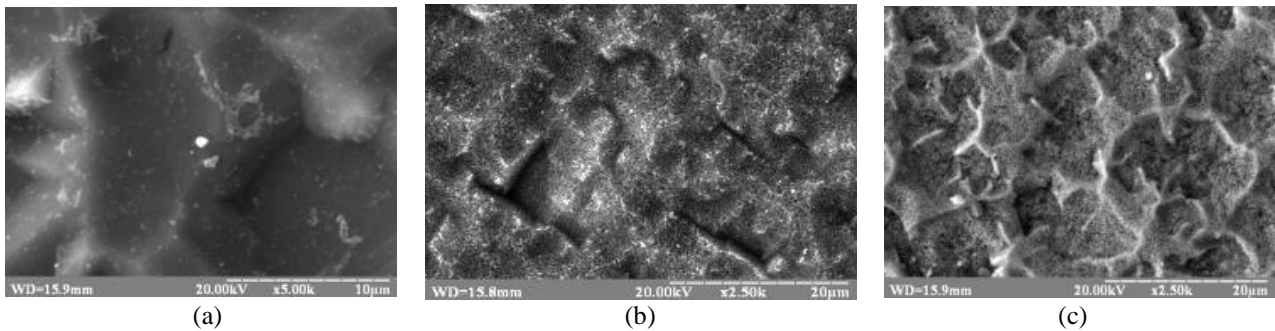
(a)   (b)   (c)

Fig. 3. SEM of the MACE Si surface after 50 min etching with different NPs (a) Au (NPs 40…50 nm, drop deposition, sample Au1), (b) Ag (10 s NPs deposition, sample Ag14), (c) Cu (sample Cu3).

It was found that the average height of obtained nanostructures was 888 nm (for 30 min) and 708 nm (for 90 min). Thus, shorter etching time results in higher NWs with an elongated shape.

The content of H_2O_2 in the second solution also had significant effect on the morphology of the etched Si surface. It was found that the smaller amount of the component (0.4 ml) leads to formation of a less etched surface as compared with the larger one (0.8 or 1.6 ml). The etched surface looks like those shown in Figs 4a and 4b, respectively.
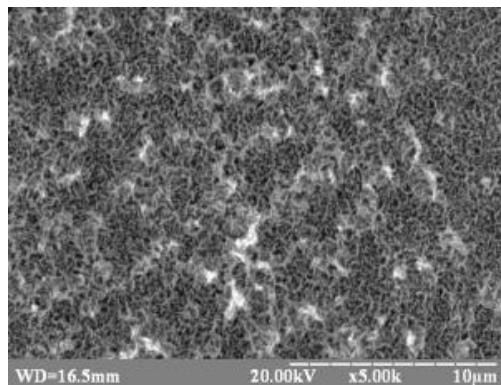
(a)
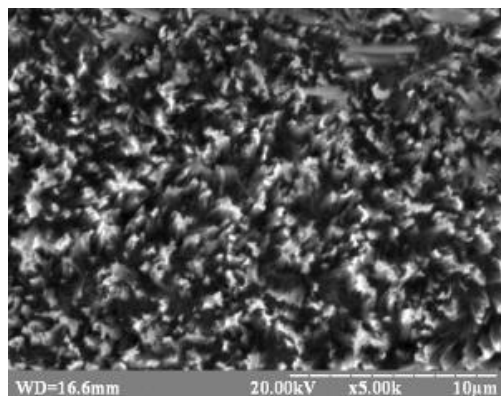
(b)

Fig. 4. SEM images of the MACE Si surface for different duration of the second stage: a) 30 min (Ag4), b) 90 min (Ag5). The content of H_2O_2 in solution was the same (0.8 ml). Ag NP deposition conditions:$AgNO_3$ – 68 mg, deposition time – 20 s.

Moreover, the difference in morphological features of surfaces etched at different H_2O_2 content, gradually decreases with etching time increasing from 30 to 150 min. In the case of one-stage MACE with Cu nitrate, the etching time increase provides visibly deeper relief.

3.4. Sensor application of Si nanostructures

Si nanostructures have been widely used in sensing applications for the recent 20 years. Special interest to MACE structures is induced by a simple, cheap and well-controlled technical process as well as by possible participation of metal NPs in the detection process.

In this work, sensitivity of Si nanostructures to hydrogen peroxide and glucose (*via* glucose oxidase reaction) was evaluated.

For sensor properties measurements, 0.5 ml solution drop was placed between contacts by using hydrophobic properties of Si as shown in Fig. 5. For glucose measurements, 0.1 ml of glucose water solution was added to 0.5 ml glucose oxidase solution (>10 IU/ml).

The current-voltage (*I–V*) curves of resistor structure were measured from 1 to 20 V. *I–V* curves for all the samples are linear with a slope changing with analyte concentration changes (Fig. 6).

Initially, Cu and Ag had been chosen because of their catalyst properties towards glucose (Cu) and hydrogen peroxide (Ag) decomposition. However, in this work the best results for both Cu and Ag were obtained for the samples with removed NPs. It was shown that the removal of Ag NPs increases structures sensitivity to H_2O_2 from 0.25 mA/V·% [28] to more than 2.5 mA/V·% (Table 2).
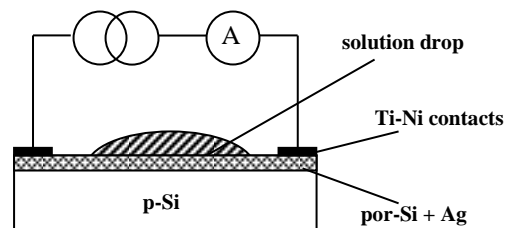

Fig. 5. Sensor measurement scheme. 0.5 ml solution drop is deposited between contacts using hydrophobic properties of melanin.
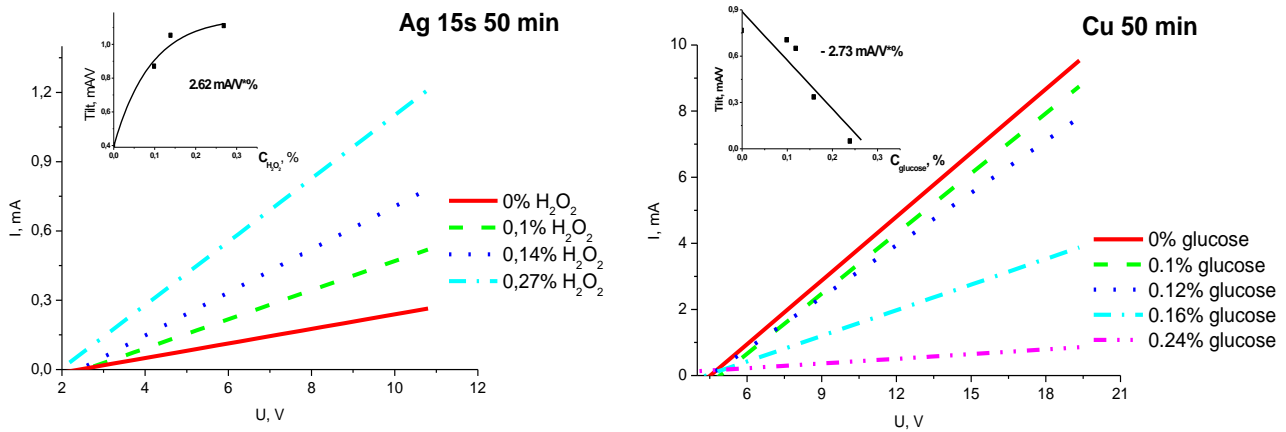
Fig. 6. *I–V* curves of the best samples for H₂O₂ detection (left) – sample Ag16 (15 s first stage, 50 min second stage), and glucose detection (right) Cu3 (one-stage 50 min, fast cleaning) – right) with tilt dependence on concentration in the inset.

Comparing to other porous silicon based sensors [29, 30], our samples demonstrate almost the same limit of detection (LOD) and range (Table 3). On the other hand, they benefit simplicity of production and low-cost technology.

Nonetheless, sensing selectivity depends on material of NPs. Samples prepared with Ag NPs are more sensitive to hydrogen peroxide, and *I–V* slope increases with concentration growth (Fig. 6a). Samples prepared with Cu NPs are more sensitive to glucose, and *I–V* slope decreases with the concentration growth (Fig. 6b). Samples with Au NPs are sensitive to both analytes. These phenomena need further investigation, but one could suggest that it can be related to small amounts of metal residue in caves of nanopores either with different pores shape or dimensions.

The increase of duration of both stages of MACE enhances the sensitivity of sensors. It may happen due to increasing pore density and depth, *i.e.*, surface area and surface states quantity.

3.5. Photovoltaic application of Si nanostructures

Si MACE nanostructures are used in solar cells to improve the current characteristics of the devices through more efficient light trapping. However, the value of optical reflection from a structured surface strongly depends on the conditions of the MACE process: the duration of both stages (Fig. 7a) and the chemical composition of both solutions (Fig. 7b). For the most of etching modes, the reflection coefficient of Si surface is much lower than that for flat Si substrate and lies between 11 and 20% at the wavelength 600 nm.

As one can see from Fig. 7a, the deposition time of Ag NPs has a significant influence on the reflection spectra of the MACE Si surface (at the same duration of the second stage). It was shown that for both etching durations (90 or 150 min), the reflection coefficient increases, as the duration of Ag-deposition changes from 10 to 60 s.

Table 3. Comparison of different sensors based on porous silicon.

Sensor type	LOD, mg/dl	Range, mg/dl
Optical porous silicon based sensor [29]	6	18...540
Amperometric porous silicon sensor [30]	0.36	3.6...9000
Resistor-like porous silicon sensor (this study)	20	100...240

Table 2. Dependence of sensor sensitivity on sample preparation conditions.

Sample preparation conditions				Sensitivity, mA/V·%	
				Hydrogen peroxide	Glucose
Au1	Au (40…50 nm)	50		2.56	1.23
Ag13	Ag (cleaned)	10	40	0.36	–
Ag14			50	0.92	–
Ag16		15	40	1.02	–
Ag17			50	2.62	–
Cu2	Cu (cleaned)	40		–	–2.25
Cu3		50		–	–2.73

This growth is characterized by non-gradual behavior: the reflection coefficient increases by 2-3% at the transition from 10 to 40 s, while Ag deposition for 60 s results in much more sharp increase (by 7%). The obtained results can be explained by structural studies shown in Fig. 2. The minimum reflection value (11% at the wavelength 600 nm) is observed for the first stage duration of 10 s, when a pure Si MACE surface is synthesized. With the increase in Ag NPs deposition time to 40 s, there is precipitation of another phase (Ag) at the Si surface, so the minimum reflection value increases up to 13% (at the wavelength 600 nm). The highest reflectance values (20% at the same wavelength) were obtained for Ag deposition duration close to 60 s, which is explained by the presence of Ag dendrites on the MACE Si surface. At the same duration of the first stage, the increase of second-stage duration from 90 to 150 min leads to enlarging optical reflection (Fig. 7a).

This is explained by the fact that lateral branching, which appeared during the longer etching process, results in a significant increase of distance between Si nanostructures and in the change of direct-standing shape of gaps between them (Fig. 4). So, this MACE modification of Si causes less efficient light trapping. It should be noted that for Ag deposition time close to 10 s the difference in reflective properties for 90 min- and 150 min-etched Si is maximum (influence of pure Si surface), and for 60 s the reflection value for these samples is almost the same (influence of Ag dendrites).

The influence of chemical composition of both MACE solutions is presented in Fig. 7b. As can be seen from the reflectance spectra, the optimal content of $AgNO_3$ in the first solution (H_2O_2 content in the second solution was constant and equal to 0.8 ml) is 68 mg, since there is a minimum reflection under these conditions (approximately 16% at the wavelength 600 nm). The decrease in $AgNO_3$ content twice (34 mg) provides only slightly more light reflection at the same

wavelength 600 nm (about 17%), while in the long-wave range the opposite ratio is observed. Taking into account the integral reflection over a wide spectrum, both concentrations of $AgNO_3$ can be used for the synthesis of solar cells. This can be explained by appearance of Ag inclusions even during the first stage of 20 s, as explained in the previous section.

The influence of H_2O_2 content in the second solution on the reflective properties of the MACE Si surface was revealed ($AgNO_3$ content in the first solution was constant – 68 mg) (Fig. 7b). In particular, it was shown that a more concentrated etching solution provides a gradual increase in the reflection coefficient from 13 up to 17% at the wavelength 600 nm. Being based on structural studies mentioned above, this dependence is associated with a larger amount of etched-off Si and formation of NWs separated by large gaps of indirect shape. This MACE modification of the Si substrate leads to an increase in light reflection. Hence, the content of hydrogen peroxide at the level of 0.4 ml is optimal for PV application, because it provides the minimum optical reflectance (13% at the wavelength 600 nm).

Si solar cells were fabricated on the obtained MACE Si substrates. The influence of technological parameters of the first and second MACE stages on photovoltaic properties was studied (Fig. 8). As one can see from I–V curves of solar cells, the MACE process mainly affects the short-circuit current density (J_{sc} could be changed by the factor of 5 at the first stage, and by the factor of 2.5 at the second one) and causes only slight changes of the open-circuit voltage (the variation of V_{oc} value for both stages is about 10%). It is known that photovoltaic current in PV devices is defined by the number of absorbed photons and the number of charge carriers that have overcome the p-n junction. In this work, the clear correlation between short-circuit current and reflection coefficients for various MACE processes was observed. Thus, the PV characteristics of Si solar cells were investigated in terms of the reflective properties of MACE Si surface.
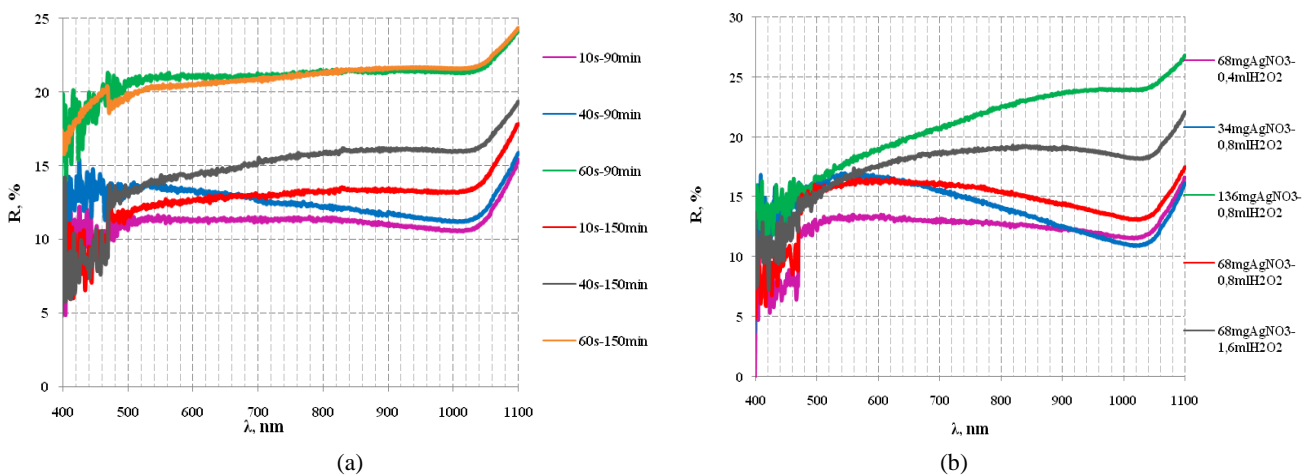

Fig. 7. Reflectance spectra of MACE Si surface for different durations of first/second stages in MACE process: 10 s/90 min, 40 s/90 min, 60 s/90 min, 10 s/150 min, 40 s/150 min, 60 s/150 min (a) and for different content of solutions at the first/second stages in MACE process: 68 mg $AgNO_3$/0.4 ml H_2O_2, 34 mg $AgNO_3$/0.8 ml H_2O_2, 68 mg $AgNO_3$/0.8 ml H_2O_2 , 136 mg $AgNO_3$/0.8 ml H_2O_2, 68 mg $AgNO_3$/1.6 ml H_2O_2(b).

Dusheiko M.G., Koval V.M., Obukhova T. Yu. Silicon nanowire arrays synthesized using the modified MACE …

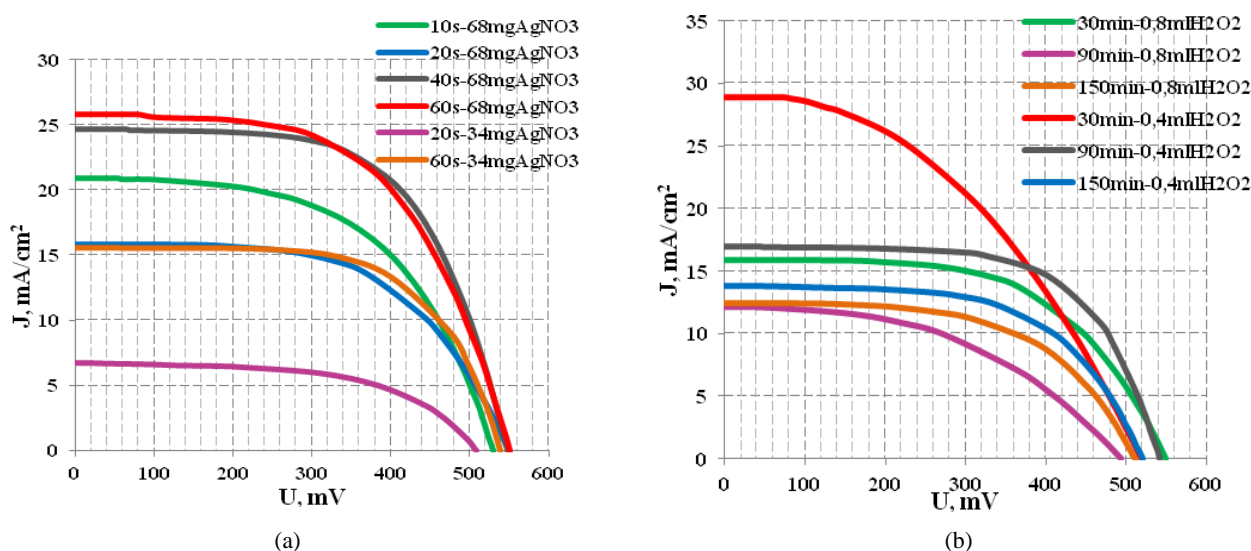(a)   (b)

Fig. 8. *I–V* characteristics of MACE solar cells for various technological conditions of the first stage in MACE process: 10 s/68 mg AgNO$_3$, 20 s/68 mg AgNO$_3$, 40 s/68 mg AgNO$_3$, 60 s/68 mg AgNO$_3$, 20 s/34 mg AgNO$_3$, 60 s/34 mg AgNO$_3$ (a) and the second stage in MACE process: 30 min/0.8 ml H$_2$O$_2$, 90 min/0.8 ml H$_2$O$_2$,150 min/0.8 ml H$_2$O$_2$, 30 min/0.4 ml H$_2$O$_2$, 90 min/0.4 ml H$_2$O$_2$, 150 min/0.4 ml H$_2$O$_2$ (b).

During the first stage of MACE process for photovoltaic application, the technological parameters of the second stage were not changed (etching 30 min, hydrogen peroxide amount 0.8 ml). For any content of AgNO$_3$, the following dependence of PV parameters on the deposition time of Ag NPs is observed: the short-circuit current density is greater for regimes when dendrites appear (40…60 s) than for regimes without them (10…20 s). Thus, increasing the deposition time of Ag NPs from 10...20 up to 40...60 s allowed us to increase the short-circuit current density from 16...21 up to 25...26 mA/cm^2 for AgNO$_3$ content equal to 68 mg. It should be noticed that with the longer duration of the first stage, the optical reflection increases (Fig. 7a), because large branched Ag dendrites appear at the surface (Fig. 2c). However, the process of PV-manufacturing is preceded by operation to remove the Ag residues from the MACE Si surface. The observed improvement in the PV characteristics is apparently due to formation of a specific Si nanostructure beneath the dendrites, which significantly reduces the reflective properties of the MACE surface. For both regimes at the first stage of MACE process (with and without dendrites), lowering the Ag nitrate content from 68 down to 34 mg results in deterioration of solar cell current characteristics by several times.

Comparison of the obtained results with optical reflection spectra (Fig. 7b) revealed that the reflectance properties of MACE surface for both contents of AgNO$_3$ slightly differ. It means that a lower concentration of nanoparticle catalysts on Si surface in MACE process results in a fewer number of NWs, thereby reducing the amount of free current carriers.

During the second stage of MACE process for photovoltaic application, the technological parameters of the first stage were not changed (deposition duration 20 s,

AgNO$_3$ amount 68 mg). For both concentrations of hydrogen peroxide, the following dependence of PV parameters on the deposition time of Ag NPs is observed: the short-circuit current density decreases as the etching time increases within the range 30…150 min (from 16 up to 12 mA/cm^2 and from 29 to 14 mA/cm^2 for hydrogen peroxide content 0.8 ml and 0.4, respectively). It should be noted that the currently available solar cells obtained in a similar way (MACE and diffusion process), show the short-circuit current at the level of 22...25 mA/cm^2 [29]. The observed tendency is fully consistent with the results of structural and reflective properties of the MACE surface (Figs 4 and 7). Indeed, the increase of etching time and concentration of the etchant leads to a clear increase in optical reflectance, which is due to the specific surface morphology of the MACE Si. So, we can conclude that the non-excessively etched MACE surface is preferred for PV-applications. The MACE synthesis of tightly packed NWs with small gaps of direct shape contributes to a more efficient light trapping.

4. Conclusions

In this work, the MACE process has been investigated in terms of its efficiency in PV and sensor applications. Results of studying surface morphology and roughness analysis show that nanostructure morphology may be controlled in a wide limits by the etching time, amount of components in solution and NPs material. Resistor-like sensors with nanostructured Si fabricated in this work demonstrate sensitivity up to 2.5...2.75 mA/V·% to hydrogen peroxide and glucose. Removal of metal NPs results in better sensitivity, although the type of metal could provide selectivity between hydrogen peroxide and glucose. The influence of technological parameters (duration and content of solutions) in two-stage MACE process on the photovoltaic characteristics has been

Dusheiko M.G., Koval V.M., Obukhova T. Yu. Silicon nanowire arrays synthesized using the modified MACE …

studied in terms of structural and reflective properties of MACE surface. It has been shown that application of the MACE process improves the short-circuit current density in Si solar cells (up to 29 mA/cm^2).

References

1. Hochbaum A.I., Fan R., He R., Yang P. Controlled growth of Si nanowire arrays for device integration. *Nano Lett.* 2005. **5**, Issue 3. P. 457–460. https://doi.org/10.1021/NL047990X.

2. Song T., Lee S.-T., Sun B. Silicon nanowires for photovoltaic applications: The progress and challenge. *Nano Energy*. 2012. **1**, Issue 5. P. 654–673. https://doi.org/10.1016/j.nanoen.2012.07.023.

3. Charrier J., Najar A., Pirasteh P. Study of optical absorbance in porous silicon nanowires for photovoltaic applications. *Appl. Surf. Sci.* 2013. **283**. P. 828–832. https://doi.org/10.1016/J.APSUSC.2013.07.026.

4. Miranda A., Santiago F., Pérez L.A., Cruz-Irisson M. Silicon nanowires as potential gas sensors: A density functional study. *Sensors and Actuators B.* 2017. **242**. P. 1246–1250. https://doi.org/10.1016/j.snb.2016.09.085.

5. Chen S., Berg A., Carlen E.T. Sensitivity and detection limit analysis of silicon nanowire bio(chemical) sensors. *Sensors and Actuators B.* 2015. **209**. P. 486–489. https://doi.org/10.1016/j.snb.2014.12.007.

6. Canevali C., Alia M., Fanciulli M., Longo M., Ruffo R., Mariab C.M. Influence of doping elements on the formation rate of silicon nanowires by silver-assisted chemical etching. *Surface & Coatings Technology*. 2015. **280**. P. 37–42. https://doi.org/10.1016/j.surfcoat.2015.08.013.

7. Abdur-Rahman E., Alghoraibi I., Alkurdi H. Effect of isopropyl alcohol concentration and etching time on wet chemical anisotropic etching of low-resistivity crystalline silicon wafer. *Int. J. Anal. Chem*. 2017. **2017**. P. 1–9. https://doi.org/10.1155/2017/7542870.

8. Amri C., Ouertani R., Hamdi A., Ezzaouia H. Effect of silver-assisted chemical vapor etching on morphological properties and silicon solar cell performance. *Materials Science in Semiconductor Processing*. 2017. **63**. P. 176–183. https://doi.org/10.1016/j.mssp.2017.02.019.

9. Lee Y., Kim H., Hussain S.Q. *et al*. Study of metal assisted anisotropic chemical etching of silicon for high aspect ratio in crystalline silicon solar cells. *Materials Science in Semiconductor Processing*. 2015. **40**. P. 391–396. https://doi.org/10.1016/j.mssp.2015.07.011.

10. Ghafarinazari A., Mozafari M.A. Systematic study on metal-assisted chemical etching of high aspect ratio silicon nanostructures. *Journal of Alloys and Compounds*. 2014. **616**. P. 442–448. https://doi.org/10.1016/j.jallcom.2014.07.044.

11. Smith Z.R., Smith R.L., Collins S.D. Mechanism of nanowire formation in metal assisted chemical etching. *Electrochimica Acta*. 2013. **92**. P. 139–147. https://doi.org/10.1016/j.electacta.2012.12.075.

12. Bachtouli N., Aouida S., Bessais B. Formation mechanism of porous silicon nanowires in HF/AgNO$_3$ solution. *Microporous and Mesoporous Materials*. 2014. **187**. P. 82–85. https://doi.org/10.1016/j.micromeso.2013.11.048.

13. Tsujino K., Matsumura M. Morphology of nanoholes formed in silicon by wet etching in solutions containing HF and H$_2$O$_2$ at different concentrations using silver nanoparticles as catalysts. *Electrochimica Acta*. 2007. **53**, P. 28–34. https://doi.org/10.1016/j.electacta.2007.01.035.

14. Kato Yu., Adachi S. Fabrication and optical characterization of Si nanowires formed by catalytic chemical etching in Ag$_2$O/HF solution. *Appl. Surf. Sci*. 2012. **258**, Issue 15. P. 5689–5697. https://doi.org/10.1016/j.apsusc.2012.02.063.

15. Lajvardi M., Eshghi H., Izadifard M., Ghazi M.E., Goodarzi A. Effects of silver and gold catalytic activities on the structural and optical properties of silicon nanowires. *Physica E*. 2016. **75**. P. 136–143. https://doi.org/10.1016/j.physe.2015.09.007.

16. Cichoszewski J., Reuter M., Schwerdt F., Werner J.H. Role of catalyst concentration on metal assisted chemical etching of silicon. *Electrochimica Acta*. 2013. **109**. P. 333–339. https://doi.org/10.1016/j.electacta.2013.07.079.

17. Backes A., Bittner A., Leitgeb M., Schmid U. Influence of metallic catalyst and doping level on the metal assisted chemical etching of silicon. *Scripta Materialia*. 2016. **114**. P. 27–30. https://doi.org/10.1016/j.scriptamat.2015.11.014.

18. Romano L., Vila-Comamala J., Jefimovs K., Stampanoni M. Effect of isopropanol on gold assisted chemical etching of silicon microstructures. *Microelectronic Engineering*. 2017. **177**. P. 59–65. https://doi.org/10.1016/j.mee.2017.02.008.

19. Sahoo M.K., Kale P.G. Micro-Raman study of growth parameter restraint for silicon nanowire synthesis using MACE. *Superlattices and Microstructures*. 2019. **135**. P. 106289. https://doi.org/10.1016/j.spmi.2019.106289.

20. Singh N., Sahoo M.K., Kale P.G. Effect of MACE parameters on length of porous silicon nanowires (PSiNWs). *J. Cryst. Growth*. 2018. **496–497**. P. 10–14. https://doi.org/10.1016/j.jcrysgro.2018.05.019.

21. Han H., Huang Z., Lee W. Metal-assisted chemical etching of silicon and nanotechnology application. *Nano Today*. 2014. **9**, Issue 3. P. 271–304. https://doi.org/10.1016/j.nantod.2014.04.013.

22. Chartier C., Bastide S., Levy-Clement C. Metal-assisted wet chemical etching of crystalline silicon. *Proc. 22nd Europ. Photovoltaic Solar Energy Conf*. 3-7 September 2007. Milan, Italy. P. 1231–1234.

23. Toor F., Miller J.B., Davidson L. M., Nichols L. Nanostructured silicon *via* metal assisted catalyzed etch (MACE): chemistry fundamentals and pattern engineering. *Nanotechnology*. 2016. **27**. P. 412003. https://doi.org/10.1088/0957-4484/27/41/412003.

24. Huang Z., Zhang X., Reiche M. *et al.* Extended arrays of vertically aligned sub-10 nm diameter [100] Si nanowires by metal-assisted chemical etching. *Nano Lett.* 2008. **8**, Issue 9. P. 3045–3051. https://doi.org/10.1021/nl802324y.

25. Megouda N., Hadjersi T., Szunerits S., Boukherroub R. Electroless chemical etching of silicon in aqueous $NH_4F/AgNO_3/HNO_3$ solution. *Appl. Surf. Sci.* 2013. **284**. P. 894–899. https://doi.org/10.1016/j.apsusc.2013.08.033.

26. Rabha M. B., Khezami L., Jemai A.B. *et al.* Surface passivation of silicon nanowires based metal nano-particle assisted chemical etching for photovoltaic applications. *J. Cryst. Growth.* 2017. **462**. P. 35–40. https://doi.org/10.1016/j.jcrysgro.2017.01.021.

27. Cao Y., Zhou Y., Liuz F. *et al.* Progress and mechanism of Cu assisted chemical etching of silicon in a low Cu^{2+} concentration region. *ECS J. Solid State Sci. Technol.* 2015. **4**, Issue 8. P. 331–336. https://doi.org/10.1149/2.0191508jss.

28. Obukhova T., Dusheiko M., Tymoshenko O., Chubenko Y. Resistor-like porous silicon glucose sensor with silver nanoparticles. *Int. Journal of Electrical, Electronics and Data Communication (IJEEDC).* 2019. **7**, No 9. P. 1–3. http://iraj.doionline.org/dx/IJEEDC-IRAJ-DOIONLINE-16148.

29. Basu D., Sarkar T., Sen K., Hossain S. M., Das J. Multi-parametric optical glucose sensor based on surface functionalized nano-porous silicon. *IEEE Sensors J.* 2018. **18**, Issue 24. P. 9940–9947. https://doi.org/10.1109/JSEN.2018.2872846.

30. Ensafi A.A., Abarghoui M.M., Rezaei B. A new non-enzymatic glucose sensor based on copper/porous silicon nanocomposite. *Electrochimica Acta.* 2014. **123**. P. 219–226. https://doi.org/10.1016/j.electacta.2014.01.031.

31. Ray S., Ghosh S., Ghosh H. *et al.* Fabrication of nanowire on micro textured crystalline silicon wafer before and after diffusion process: A comparative study of solar cell performance. *Materials Today: Proc.* 2017. **4**. P. 12678–12683. https://doi.org/10.1016/j.matpr.2017.10.082.

Authors and CV

Mykhailo G. Dusheiko, born in 1961, defended his Diploma of Physicist in 1983 at the Taras Shevchenko National University of Kyiv. Principal Engineer at the Department of Microelectronics, National Technical University of Ukraine "Igor Sikorsky Kyiv Polytechnic Institute". Authored over 90 publications and 5 patents. The area of his scientific interests includes physics and technology of semiconductor materials for optoelectronic and sensor devices (sensors of chemical and physic-cal parameters, solar cells, photodetectors, *etc.*). E-mail: mgd61@ukr.net, https://orcid.org/0000-0003-2267-6637

Viktoriia M. Koval, born in 1980, defended his PhD thesis in Technical Sciences (Solid-State Electronics) in 2011 at the National Technical University of Ukraine "Kyiv Polytechnic Institute". Associate Professor at the Department of Microelectronics of the same university. Authored over 50 publications and 8 textbooks. The area of her scientific interests includes semiconductor nanomaterials and nano-technology in sensors and solar cells. https://orcid.org/0000-0002-3898-9163

Tetiana Y. Obukhova, born in 1983, defended her PhD thesis in Technical Science (Solid-State Electronics) in 2012 at the National Technical University of Ukraine "Kyiv Polytechnic Institute". Associate professor of the Department of micro- and nanoelectronics of the same university. Authored over 20 publications. The area of his scientific interests includes technology, physics and applications of porous semiconductor materials, organic-inorganic hybrid structures and devices based on them. https://orcid.org/0000-0001-6415-4461.

Author contribution

Dusheiko M.G.: Supervision, Conceptualization, Resources.

Koval V.M.: Investigation, Visualization, Writing - Original Draft, Review & Editing.

Obukhova T.Yu.: Investigation, Validation, Writing - Original Draft.

Метал-стимульований хімічний синтез масивів кремнієвих нанониток: використання у хімічних сенсорах та сонячних елементах

М.Г. Душейко, В.М. Коваль, Т.Ю. Обухова

Анотація. У роботі досліджено вплив технологічного процесу метал-стимульованого хімічного травлення на морфологію поверхні та електрофізичні властивості отриманих нанорозмірних структур. Було показано, що отримані структури мають високу площу поверхні та можуть використовуватися як у сенсорах, так і у сонячних елементах. Було продемонстровано покращення характеристик сонячних елементів у результаті використання процесу метал-стимульованого травлення, зокрема значне підвищення струму короткого замикання (до 29 мА/см^2). Також була доведена можливість детектування перекису водню та глюкози (ферментним методом) за допомогою резистивних сенсорів з наноструктурованим кремнієм як активного шару з чутливістю до 2.5…2.75 мА/В·%.

Ключові слова: метал-стимульоване хімічне травлення, кремнієві нанонитки, сенсор, сонячний елемент.

Dusheiko M.G., Koval V.M., Obukhova T. Yu. Silicon nanowire arrays synthesized using the modified MACE …